The synergistic fouling of ceramic membranes by particles and natural organic matter fractions using different surface waters in South Africa

Moyo, Welldone; Chaukura, Nhamo; Motsa, Machawe M.; Mthombeni, Nomcebo H.; Msagati, Titus A.M.; Mamba, Bhekie B.; Heijman, Sebastiaan G.J.; Nkambule, Thabo T.I.

DOI
10.22079/JMSR.2020.127635.1384

Publication date
2021

Document Version
Final published version

Published in
Journal of Membrane Science and Research

Citation (APA)
Moyo, W., Chaukura, N., Motsa, M. M., Mthombeni, N. H., Msagati, T. A. M., Mamba, B. B., Heijman, S. G. J., & Nkambule, T. T. I. (2021). The synergistic fouling of ceramic membranes by particles and natural organic matter fractions using different surface waters in South Africa. *Journal of Membrane Science and Research*, *7*(2), 125-137. https://doi.org/10.22079/JMSR.2020.127635.1384

Journal of Membrane Science & Research

journal homepage: www.msrjournal.com

Research Paper

The Synergistic Fouling of Ceramic Membranes by Particles and Natural Organic Matter Fractions using Different Surface Waters in South Africa

Welldone Moyo [1], Nhamo Chaukura [1,2], Machawe M. Motsa [1], Nomcebo H Mthombeni [3], Titus A.M Msagati [1], Bhekie B. Mamba [4], Sebastiaan G.J Heijman [5], Thabo T.I Nkambule [1,*]

[1] *Institute for Nanotechnology and Water Sustainability (iNanoWS), University of South Africa (UNISA), Johannesburg, South Africa*
[2] *Department of Physical and Earth Sciences, Sol Plaatje University, Kimberley, South Africa*
[3] *Department of Civil and Chemical Engineering, University of South Africa (UNISA), Johannesburg, South Africa*
[4] *College of Science, Engineering and Technology, University of South Africa (UNISA), Johannesburg, South Africa*
[5] *Department of Civil Engineering and GeoSciences, Technical University of Delft, Delft, the Netherlands*

Article info

Received 2020-05-14
Revised 2020-06-11
Accepted 2020-07-05
Available online 2020-07-05

Keywords

Fluorescent organic matter
Membrane fouling resistance
Modified fouling index
Particulate organic matter
Synergistic fouling

Highlights

- Fouling development and mechanism is demonstrated using 'real' water samples.
- Contribution of inorganic particles on the synergistic fouling is demonstrated.
- Physico-chemical characteristics of feed water on fouling development are described.

Graphical abstract

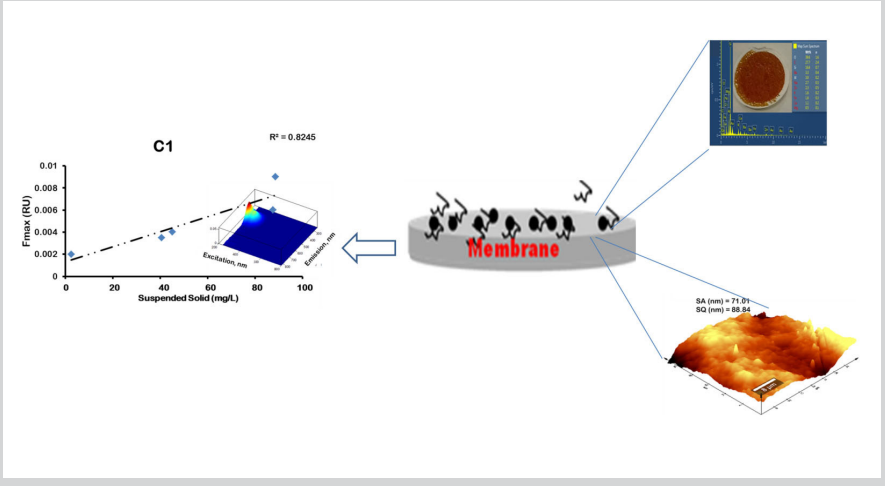

Abstract

This study demonstrates the fundamental differences in fouling development and mechanisms of unfiltered and 0.45 µm pre-filtered water samples on ceramic membranes. Robust characterization of the feed waters was conducted using gravimetric analysis, optical methods and modeling techniques. UV_{254} removal and suspended solids (SS) for the unfiltered samples presented a strong correlation (R^2 = 0.87). Further, SS exhibited strong correlations with fluorescent fractions (R^2 = 0.82; 0.81 and 0.74 for C1; C2 and C3, respectively). This observation confirmed the significance of inorganic particles in the development of a combined fouling layer with fluorescent organic components. The fouling development rate for water sampled from Plattenburg Bay (PL) was higher than the rest of the 0.45 µm pre-filtered samples. This was attributed to the low conductivity (175 $\mu S.m^{-1}$) of the water sample, translating to a low ionic strength environment. Samples collected from Hermanus River (HL) and Lepelle River (OL) had similar SS quantity (87.6 mg/L and 88.4 mg/L, respectively), and modified fouling index (MFI) values for raw samples were 6625 and 8060 s/L^2, respectively, despite a very large difference in the content of organic matter (22.67 mg/L.C and 9.81 mg/L.C). This could be due to organic matter attaching onto the surface of particles and reducing the adsorption of NOM within membrane pores and/or onto the membrane active layer. This study demonstrated the extent of in situ background electrolytes, foulant concentration, foulant-foulant interactions, foulant-membrane interaction and physicochemical properties of feed stream on fouling development and mechanisms.

1. Introduction

The effective operation of drinking water treatment systems is continuously deteriorating owing to the accumulation of natural organic matter (NOM) in surface source waters across the world [1,2]. As a result, most drinking water treatment plants, mainly in developing countries, are operating at reduced capacity for the removal of NOM. Residual NOM in drinking water causes poor organoleptic properties, bacterial proliferation in

* Corresponding author: nkambtt@unisa.ac.za (T.T.I. Nkambule)

DOI: 10.22079/JMSR.2020.127635.1384

the distribution network, biofilm formation, formation of disinfection by-products (DBPs) and membrane fouling [3]. The conventional treatment processes employed by most water treatment plants, particularly in developing countries, include disinfection, filtration, sedimentation and coagulation/flocculation. However, these traditional unit processes do not efficiently remove NOM (around 35% at conventional pH) [4,5]. Therefore modifications of the existing NOM removal methods and or new unit processes are needed. Such methods could include adsorption, catalysis including photo-catalysis and photo-Fenton catalysis, and membrane technology.

Membrane technology has great promise for the bulk remediation of organic and inorganic pollutants in water. The applications include desalination to decontaminate waters such as wetland saline water, surface water, brackish water, seawater and wastewater [7,10]. NOM is one of the foulants that adversely affects low pressure membranes [3]. NOM is composed of particulate organic matter (POM) and dissolved organic matter (DOM). Although classifying organic matter as POM or DOM is problematic, the generally accepted distinction is that DOM is the size fraction below 0.45 µm [11]. On the one hand, DOM is composed of complex mixtures of fulvic and humic acids, proteins and simple and complex polysaccharides with varying functional groups and varying molecular weights [12]. On the other hand, POM consists of heterogeneous polymeric organic substances, inorganic particles, organic particles, living microorganisms, and organic-inorganic composites [10]. The study of combined membrane fouling due to POM/DOM coexisting with inorganic particles is increasingly attracting research attention [13,15]. Inorganic particles of interest include clays, silt, and precipitated crystals such as iron and aluminium oxyhydroxides [3,16–18]. These particles are intentionally added or naturally present. Fouling due to inorganic particles acting alone is not severe, and their deposition on the membrane is reversible and can be easily removed by physical means [13,19]. However, the presence of inorganic particles aggravates membrane fouling by NOM. For instance, the presence of inorganic particles exacerbated membrane fouling by NOM representative model compounds i.e., bovine serum albumin (BSA), sodium alginate (SAL) and humic acid (HA) [15,20–22]. Also, the size and concentration of inorganic particles play a role on the severity of NOM fouling. Tian et al., (2013) [13] reported that the quantity of SiO_2 particles (0.5 – 10 µm and 45 µm, size ranges) in the concentration range 10 – 50 mg/L had a linear relation with the extent of membrane fouling by NOM. Notwithstanding these and other research efforts, the extent of combined fouling on ceramic membranes by POM/DOM and inorganic particles found in "real" waters is not widely reported.

Traditionally, polymeric membranes have dominated the membranes market due to their cost advantage over ceramic membranes [8]. However, they suffer many drawbacks such as poor chemical stability, low thermal resistance, diminished mechanical robustness, a short life span, and limited recyclability [9]. Ceramic membranes are porous inorganic oxides commercially available as zirconia, titania (TiO_2), alumina, and more recently silicon carbide [10]. Inherent in the TiO_2 active layer of the membranes is the presence of the –OH groups, these groups enhance the hydrophilic character of the membranes and limit membrane fouling by reducing hydrophobic interactions between the foulants and active layer of the membrane [23]. Further, they have high selectivity and stability at elevated temperatures even in chemically aggressive environments [24,25]. Ceramic membranes have been introduced to the water industry close to two decades ago [72], however, research on the fouling of ceramic membranes by POM/DOM using 'real' samples is not well researched. Therefore, more research is required to comprehend the fouling mechanisms of ceramic membranes in order to fully exploit its advantages and advance its use in the water industry.

Optical methods, for instance fluorescence excitation emission matrix (FEEM) spectroscopy, ultraviolet-visible (UV-Vis) spectroscopy and optical indices such as specific ultraviolet absorbance (SUVA) and slope ratios (S_R) are widely used to characterize NOM and its fouling behavior on membranes [26–28]. Relative to DOM, POM is preferentially enriched with labile substrates for example amino acids [10]. Therefore, compositional differences and dynamics between DOM and POM could be assayed by optical methods such as FEEM. This method fingerprints and quantifies the compositional changes of fluorescent fractions of NOM. The data could be used to elucidate POM/DOM interactions with inorganic particles *in situ* and their influence on fouling of membranes as well as the produced water quality.

Previous studies report that operating parameters such as cross flow, flux and recovery are major factors responsible for the severity of fouling [29–31], and the key factors causing severe fouling are the characteristics of feed water [32,33]. This has necessitated the wide application of fouling prediction tools such as modified fouling index (MFI), fouling models and silt density index (SDI) [20,22]. Early application of MFI was for microfiltration membranes operated at dead end mode [34]. Considerable research has extended its application to nanofiltration membranes operated at cross flow mode [22,35]. Prior research has shown that MFI varies linearly with feed stream concentration, and therefore it is postulated to present the actual fouling behavior due to feed stream concentration [22]. Pretreatment requirements as determined by the utilization of the MFI method save time and resources needed in conducting pilot studies. However, many studies have concentrated on determining MFI using model NOM compounds and model particles in synthetic water [22,35]. Therefore the application of MFI for the prediction of fouling of 'real' waters on ceramic membranes deserves investigation.

The source waters in South Africa can be divided into five quality categories, namely: oligotrophic water, eutrophic water, coloured water, montaigne water, and treated waste water discharge [3]. It is expected that the water sources, catchment/anthropogenic activities and climatic conditions influence the occurrence of POM/DOM components, while the underlying geological formation determines the occurrence and distribution of inorganic particles. This study sought to: (1) investigate the contribution of spatial distribution to the character of the POM/DOM pool in selected regions of South Africa; (2) identify commonalities of specific NOM fractions and inorganic matter on the membrane fouling propensities of the different waters; and (3) systematically study the combined and individual effects of NOM, particles, and their synergistic influence on membrane fouling indices.

2. Materials and methods

2.1. Raw water sources

Five surface water sources representative of the South African water quality regions (Fig. A1) and serving water treatment plants were chosen: source water supplying the Plettenberg Bay water treatment plant (PL) namely Keurbooms River in the Southern Cape; Debose Dam (H) which supplies Violia water treatment that serves Hermanus and part of Cape Town; source water supplying Midvaal water treatment plant, namely the Vaal River (MV) in the North West province; Hezelmere River (HL) which supplies Hezelmere water treatment plant operated by Umngeni water treatment company serving the greater Umngeni municipality, and source water supplying the Mpumalanga province and parts of Polokwane city, namely Lepelle River (OL). On site, conductivity, pH, and temperature of all samples were acquired using portable field meters. All measurements were performed in triplicate.

2.2. POM-DOM and inorganic particles analysis

2.2.1. Fluorescence EEMs, UV-Vis absorbance, optical ratios and organic matter

Triplicate samples were collected and immediately couriered to the laboratory in 25-L plastic containers. Before analysis, the samples were equilibrated to 25 °C and POM immediately measured, DOM analysis was performed after filtering the raw samples through 0.45 µm GF/F filters (Whatman filters, German). UV-Vis absorbance and fluorescence EEMs were acquired using a fluorescence spectrometer (Aqualog, HORIBA, Jobin Yvon) set at 200-800 nm wavelength range. The excitation interval was set at 2 nm and the emission was recorded between 248.58-830.59 nm with an emission interval of 3.28 nm. Raman water peak area was used to calibrate and correct the measured intensities and convert to Raman units (RU) from arbitrary units (AU). This was achieved by exciting the Raman water standard at λ = 350 nm and measuring the emission readings between 248.58 to 830 nm [36]. Specific ultraviolet absorbance ($SUVA_{254}$) is the quotient of UV_{254} absorbance and *DOC*. The aromaticity (ϕ_{254}) was calculated using Equation 1 [11]:

$$\phi_{254}(\%) = 527 \times SUVA_{254} + 2.8 \quad (1)$$

S_R was calculated as the quotient of the spectral slope of 275 nm – 295 nm and 350 – 400 nm (Equation 2). A reduction in the ratio indicates an increase in molecular size [37,38].

$$S_R = \frac{Slope_{A_{275\rightarrow295}}}{Slope_{A_{350-400}}} \quad (2)$$

A total organic carbon analyser (TOC fusion, Teledyne Tekmar) was used to measure the quantity of organic matter and the rejection of organic matter (r_{OM}) was calculated (Equation 3) [39]:

$$r_{OM} = \frac{C_o - C_p}{C_o} \quad (3)$$

where, C_0 and C_p are the initial *OM* concentration in the feed stream and the collected permeate, respectively.

2.2.2. Parallel factor analysis (PARAFAC) and peak picking method for the quantification of NOM fractions

To gain further insights on the occurrence and distribution of fluorescent organic matter fractions before and after filtering with 0.45 µm filter, *PARAFAC* was used. The SOLO software which runs *PARAFAC* is in built in the Aqualog instrument and was used to identify and quantify the fluorescent fractions in the POM and DOM pool. To generate components that represent universal variance between water sources, *PARAFAC* data was obtained by pooling data from all water sources including their 0.45 µm filtered permeates. A three-components model was established and the split half criterion was used for validation [40]. The maximum fluorescence intensities (F_{max}) index was used to quantify the distribution of each component in the POM and DOM pool. The obtained fluorescence components were cross-referenced with those obtained globally by using the freely accessible OpenFlour database [41].

The traditional peak picking method was employed to identify peaks (Table A1). The relative quantity and position of the maximum peak in the particular region was also assessed from the feed and permeate sides of the unfiltered and the 0.45 µm filtered water samples.

2.2.3. Inorganic particle analysis

Raw water samples (25 L) were filtered through 0.45 µm filters. The elemental composition of the membrane and the sedimented particles were mapped using a field emission scanning electron microscope (FESEM) (JSM-IT300, JEOL, Tokyo, Japan) complemented with an energy dispersive X-ray (EDX) detector.

2.3. Membrane characterization, operation and fouling analysis

2.3.1. Substrate membranes

Purchased ceramic nanofiltration (NF) membranes obtained from Innopor, Germany, were utilised in these experiments (Fig. A2). The membranes had a disc configuration of 90 mm diameter, 2.5 mm thickness, pore size of 0.9 nm, 30 % porosity, an effective filtration area of 0.00563 m^2, a molecular weight cut off (MWCO) of 450 Da, and can withstand a pressure of up to 0.3 MPa. The top layer of the membranes was made of TiO_2. The cross-sectional morphological structure of the membranes was analysed using a scanning electron microscope (JSM-IT300, JEOL; Tokyo, Japan) (Fig. A3).

2.3.2. Contact angle and surface energetics

The contact angle (θ) was measured by using the sessile drop method [42]. In the method, three liquids with well-characterized surface tension components, namely: Milli-Q water, diiodomethane and glycerol, were used. At least ten drops per liquid were deposited on the membrane using a microlite syringe, from which θ was determined (Fig. A4). This was then used to calculate surface tension, γ^{TOT} (Equation 4) from the Liftshitz-van der Waals component (γ^{LW}) and Lewis acid–base components γ^{AB} where γ^+ and γ^- are electron donor and acceptor, respectively. The interfacial free energy of interactions between two materials (for example, solute (s) and membrane (m) in a liquid (l)) was then determined (Equation 5).

$$\gamma^{TOT} = \gamma^{LW} + \gamma^{AB} \quad (4)$$

$$\Delta G_{slm}^{TOT} = \Delta G_{slm}^{LW} + \Delta G_{slm}^{AB} \quad (5)$$

The Young-Dupree equation (Equation 6) was used to calculate γ^{LW}; γ^+ and γ^- using the measurements from θ with 3 liquids of predetermined surface tension components [14]:

$$\left(1 + \frac{\cos\theta}{r}\right)\gamma_s + 2\left(\sqrt{\gamma_s^{LW}\gamma_l^{LW}} + \sqrt{\gamma_s^+\gamma_l^-} + \sqrt{\gamma_s^-\gamma_l^+}\right) \quad (6)$$

where the membrane roughness which increases surface area is accounted for by *r*, *s* and *l* are in this case the solid surface membrane and test liquid, respectively.

2.3.3. Atomic force microscopy imaging

Surface topology was determined by using an atomic force microscope (AFM) (Alpha300, WITEc Focus Innovations, Germany) in the non-contact mode (Fig. A5). Each membrane was scanned at a constant speed of 0.5 Hz at 5 different sites of dimensions 20 µm×20 µm and averaged. Height and roughness data were determined using the in-built Nanoscope program (Nanoscope 5.30 r3 sr3, Veeco Instruments, CA).

2.3.4. Operation of filtration system

The filtration equipment consisted of a pump operated at 1100-1180 rpm circulating the feed at a cross-flow velocity of 1 m/s (Fig. A6). The membrane was housed in a circular disc module (TAMI, Germany), and the system pressurized by altering the concentrate feed valve. Measurements were run under a TMP of 3 bar and a feed flow of 175 L/h in cross flow mode. After equilibration and prior to the sampling of both the feed and permeate, membranes were conditioned for 5 min for deionised water permeability and 1 h for the permeability of water samples. In the case of surface water feed, hourly samples were collected from the feed and permeate side for 6 h. Membrane fluxes and water temperature were monitored. The flow rate was correlated to the sample mass, and the flux and temperature-corrected permeability were determined (Equations 7-10) [43]:

$$v_s = \frac{(M_{SC} - M_C)}{(T_f \times 60)/1000} \quad (7)$$

$$\Delta P = \frac{P_f + P_c}{2} \quad (8)$$

$$J = \frac{v_s}{A} \quad (9)$$

$$L_{p,20^0C} = \frac{J}{\Delta P}.\frac{\eta_T}{\eta_{20}} = \frac{J.e^{-0.0239\,(T-20)}}{\Delta P} \quad (10)$$

where v_s is the flow rate, M_{sc} and M_c is the mass (g) of the sample container plus permeate sample and the mass (g) of the empty container respectively, T_f is the temperature of water *(°C)*, ΔP is the measured TMP (bar), P_f (bar) is the feed pressure and P_c (bar) is the concentrate pressure, J is the obtained membrane flux ($Lm^{-2}h^{-1}$), A is the effective membrane filtration area, $L_{p,20^oC}$ is the permeability at 20°C ($Lm^{-2}h^{-1}bar^{-1}$) and η_{20} and η_T are the permeate viscosities at 20°C and at the measured water temperature, respectively.

2.3.4. Determination of membrane fouling, fouling resistance and mechanism

Two sets of tests were performed for each feed stream: (1) direct filtration of the raw water sample to obtain total fouling resistance, and (2) filtration of the 0.45 µm pre-filtered water samples to determine organic fouling resistance. Ultrapure water flux was determined prior to membrane filtration experiments. Thereafter, feed water samples were filtered for 6 h, with the permeate mass automatically recorded. After each run, the membrane was thoroughly rinsed under running ultra-pure water to remove any loosely bound particles, thereafter the irreversibility of membrane fouling was determined by assessing ultrapure water flux. The different fouling resistances were determined from the flux values (Equation 11):

$$R_f = \frac{TMP}{\mu J} - R_m \quad (11)$$

R_f denotes the fouling resistance due to the deposition of foulants on the membrane (m^{-1}); The trans-membrane pressure (*TMP*) (Pa) in this case was 3 bar; the dynamic viscosity of water was denoted by μ (Pa s); membrane flux was denoted by J (m^3 / (m^2 s)) and determined at the end of 6 h of filtration to calculate fouling resistance; and ultrapure water flux (m^{-1}) was used to obtain the intrinsic membrane resistance R_m.

Similarly, intrinsic membrane resistance (R_m) was determined by measuring the ultra-pure water flux at the onset of the experiment. Thereafter, the total resistance (R_t) of the membranes was obtained by filtering for 6 h the various feed streams of the surface waters, and the permeate mass was

recorded at 5 min intervals. The normalized form (R_f/R_m) was used to express the total fouling resistance. Further, the fouling potential of each type of water was obtained by comparing the fouled-membrane permeability values to that of the ultrapure water.

The fouling mechanism models are provided in Supplementary information (Box A1) and elsewhere [20].

2.3.5. Membrane fouling index

Comprehensive measurement protocol of MFI in cross flow mode is found elsewhere [22,35,44]. In brevity, the gradient of the linear region of the graph (t/V) versus V provides the MFI value (Equation 12):

$$\frac{t}{V} = \frac{\eta R_m}{A\Delta P} + \underbrace{\frac{\eta \alpha C}{2\Delta P A^2}}_{MFI} V \tag{12}$$

Where t/V is the inverse flow rate, the dynamic viscosity is denoted by η, ΔP is the TMP, C denotes the concentration of particles in the feed, the deposited cake specific resistance is denoted by α, A is the area of the membrane and V is the cumulative volume.

MFI is proportional to the fouling potential and inversely proportional to TMP applied, so MFI can be a potential tool to compare fouling likelihood of different feed stream waters.

3. Results and discussion

3.1. Fundamental differences in the character of particulate and dissolved organic matter

3.1.1. The bulk parameters of particulate and dissolved organic matter

A proportionate removal of UV_{254} to organic matter removal by 0.45 µm filter was observed for H (47%: 32%), PL (4.2%: 6.7%) and HL (6.7%: 11.1%) (Table 1). There was however, a deviation by source MV, which exhibited a very low UV_{254} rejection (0.5%), compared to a 4.25% organic matter rejection. The disproportionate UV_{254} removal to organic matter removal from MV implies the organic matter from this source is largely non UV-Vis absorbing. It was interesting to note that OL had a UV_{254} removal rate of 64% despite a very low organic matter removal by the 0.45 µm filter (1.01%). This could be because the UV_{254} absorbing groups were attached to particles or were particulate in nature, suggesting POM is preferentially enriched with labile substrates such as amino acids [10]. Organic matter in natural waters represents a wide continuum from fluorescent to non-fluorescent or UV-Vis absorbing to non-absorbing matter [45]. Relative to other fluorescent functional groups, amino acids are low molecular and are largely composed of conjugated heterocyclic molecules with high UV_{254} absorbance extinction coefficients [46]. A poor correlation between organic matter removal and UV_{254} removal by the 0.45 µm was observed (R^2 = 0.07) (Fig. 1a). The non-dispersive infra-red detector (NDIR) measures the organic matter concentration of carbon which dissipates as carbon dioxide regardless of the chemical speciation, while UV_{254} only gives a measure of functional groups that fluoresce and/or absorb in the UV–Vis range [47]. UV_{254} indicates mainly humic substances, these are characterized by presence of aromatic rings which are associated with π-π* electron transitions and conjugated functional groups such as carbonyl and alkene bonds [1, 45].

Organic matter is a bulk parameter which does not provide succinct information on the chemical constituents of the organic matter. However, notably, the highest organic matter removals were samples from coastal plants: H, HL and PL (32, 11 and 6.7%, respectively), while inland plants had the least organic matter removal by the 0.45 µm filters (4.25 and 1.02% for MV and OL, respectively). High removal rates of organic matter for coastal plants suggest the type of organic matter in these plants is mainly bound to particles or is particulate in nature. The organic matter removal for coastal plants by 0.45 µm filters increased with increasing suspended solids (SS), however the inclusion of inland plants distorted this linearity and the overall correlation coefficient was poor (R^2 = 0.12) (Fig. 1b). Interesting results were observed, e.g., OL an inland source had high suspended solids content (88.4 mg/L) while HL a costal source had low SS content (25.2 mg/L) despite relatively similar organic matter content (9.81 and 8.28 mg/L.C, respectively). These results attest to the geo-spatial variability of organic matter and its complex interaction with inorganic particles.

As expected, a strong correlation existed between UV_{254} removal and reduction in aromaticity (R^2 = *0.77*) (Fig. 1c). UV_{254} indicates mainly humic substances, these are characterized by presence of aromatic rings which are associated with π-π* electron transitions and conjugated functional groups such as carbonyl and alkene bonds [1,45]. Aromaticity, in turn, is the measure or extent of conjugation [48]. When the results were pooled together, a strong correlation was observed between UV_{254} removal and suspended solids (R^2 = *0.87*) (Fig. 1d). These results show UV_{254} absorbing groups have a preferential adsorption affinity to inorganic particles.

Conductivity is a measure of the capability of water to allow electrical current to pass through, and its magnitude depends on the concentration of ions in the water. The 0.45 µm filter pores are too large to retain ions that is why there was no significant deference in either pH or conductivity between the 0.45 µm filtered and the unfiltered water for all samples. However, pH and conductivity values of coastal plants exhibited lower values compared to inland plants (Table 1). Perhaps the interplay of anthropogenic, undelaying bedrock and surficial geology influenced the levels of these parameters.

The primary results obtained in the analysis of bulk parameters have revealed the variability of NOM in the source waters in South Africa. Additionally, the POM and DOM present different characteristics whose physico-chemistry is expected to influence the nature and extent of fouling.

3.1.2. Suspended solids composition of source waters

The composition of inorganic particles after filtering through a 0.45 µm filter is shown in Fig. 2. The 0.45 µm filter pore size is big enough to allow the inorganic particles to pass through. The detected inorganic particles are a result of entrapment or complexation with bulky organic matter [10]. Silica or sand, which is ubiquitous to all surface waters, is made up of oxygen and silicon and thus was found in all samples. Again, in all samples oxygen was in higher proportions than any other element. This is because elements found in water exist as oxides [49]. It was expected that elemental carbon would be detected by the EDX scan because organic matter was retained to different extents by the 0.45 µm filter (H = 7.2 mg/L.C; PL = 1.3 mg/L.C; HL = 0.9 mg/L.C; OL = 0.1 mg/L.C and MV = 0.8 mg/L.C). The rejection could have been through sweep rejection, i.e. organic matter entrapped or adsorbed onto larger inorganic particles is retained together with these particles by size exclusion [13]. However, at this point it cannot be concluded that the detected carbon is organic. Inorganic carbon such as metal carbonates entrapped within a bulky particulate complex can contribute to the amount of carbon detected by the EDX scan [15].

Inorganic particles such as silicon, calcium, potassium, magnesium, zinc and aluminum have formed the basis of many theoretical studies concentrating on the influence of fouling by organic matter [25,28,32,50]. The focus on these elements in terms of composition and distribution *in-situ* as in this study gives realistic expectations to the nature and extent of fouling to be expected. The underlying geological formation on water sources determines the availability of inorganic elements found. Potassium, iron and aluminum were detected in all water sources. In addition, calcium and sodium were found in all water sources save for PL and OL, respectively. The characteristic reddish coloration of iron oxide was intense for OL (4.2%) than any other water source. Zinc was detected in only coastal sites (H) and (HL), while magnesium was only detected at OL and a very small percentage contribution was detected at H while all other plants had no magnesium detected. Barium was detected in all waters sources save for OL. The 0.45 µm pores are wide enough for inorganic particles to pass through, therefore the reported results are indicative not absolute.

3.1.3. Fluorescent organic matter composition of POM and DOM

The identity, intensity and location of peaks are discussed with reference to Table A1. Comparisons of the composition of the fluorescent organic matter pre and post filtering through a 0.45 µm filter are shown in Figure 3 and Table 2. Remarkably, peaks reduced in intensity after filtration for all water sources. The intensity of peak B was reduced the most by all water sources (HL - 72.4%; OL - 71.1%; H - 67.8%; PL - 34.3% and MV - 20.4%). The reduction of peak B attests to the fact that particulate organic matter is enriched with labile substrates such as amino acids [10]. Peak T and M were preferentially reduced in source HL (43% and 22.5%, respectively) and source OL (43.1% and 24.8%, respectively), while only peak T was preferentially removed compared to peak M at source H (45.3% and 3.3%, respectively). As for the other plants these peaks were least removed: PL (9.0% and 3.5%, respectively) and MV (13.8% and -2.3%, respectively). The removal rates for peaks A (OL: 21.2%; MV: 14.4%; H: 10.0%; PL: 5.7% and HL: 2.1%) and peak C (OL: 24.3%; H: 9.9%; HL: 7.6%; PL: 5.4% and MV: 2.9%) was minimal for all the plants. It is expected that the fouling development and rates attributable to peaks A (humic substances of allochtonous origin), C (combination of humic and fulvic substances) and M (humic substances of autochtonous origin) should be comparable for all plants.

Table 1
Bulk water characterization of the raw and 0.45 µm filtered water samples (n=3).

	DOC (mg/L.C)	UV (/cm)	SUVA (L/mg.cm)	ϕ_{254} (%)	S_R	Suspended Solids (mg/L)	pH	Conductivity (µS.m^{-1})
H Unfiltered	22.67 ± 0.02	0.55 ± 0.003	2.42 ± 0.01	15.55 ± 0.03	0.92 ± 0.001	87.6 ± 1.2	5.38 ± 0.5	317 ± 19
0.45µm Filtered	15.43 ± 0.03	0.29 ± 0.001	1.88 ± 0.02	12.71 ± 0.05	0.97 ± 0.002		5.39 ± 0.3	315 ± 14
PL Unfiltered	19.58 ± 0.04	0.48 ± 0.002	2.46 ± 0.01	15.76 ± 0.05	0.85 ± 0.001	45.2 ± 0.9	6.38 ± 0.1	175 ± 15
0.45µm Filtered	18.26 ± 0.02	0.46 ± 0.003	2.51 ± 0.01	16.03 ± 0.01	0.84 ± 0.001		6.41 ± 0.4	176 ± 13
HL Unfiltered	8.28 ± 0.04	0.15 ± 0.003	1.77 ± 0.02	12.13 ± 0.02	1.23 ± 0.002	25.2 ± 0.6	6.56 ± 0.3	177 ± 18
0.45µm Filtered	7.36 ± 0.03	0.14 ± 0.001	1.9 ± 0.02	13.02 ± 0.04	1.20 ± 0.003		6.51 ± 0.1	179 ± 11
OL Unfiltered	8.91 ± 0.01	0.39 ± 0.001	4.38 ± 0.01	25.88 ± 0.04	2.27 ± 0.005	88.4 ± 0.5	7.50 ± 0.2	623 ± 11
0.45µm Filtered	8.82 ± 0.03	0.14 ± 0.002	1.59 ± 0.02	11.18 ± 0.03	1.28 ± 0.006		7.48 ± 0.2	624 ± 13
MV Unfiltered	17.63 ± 0.02	0.21 ± 0.002	1.18 ± 0.02	9.02 ± 0.05	1.4 ± 0.003	40.8 ± 0.3	7.44 ± 0.3	450 ± 12
0.45µm Filtered	16.88 ± 0.02	0.21 ± 0.001	1.24 ± 0.01	9.33 ± 0.04	1.2 ± 0.001		7.47 ± 0.3	448 ± 10

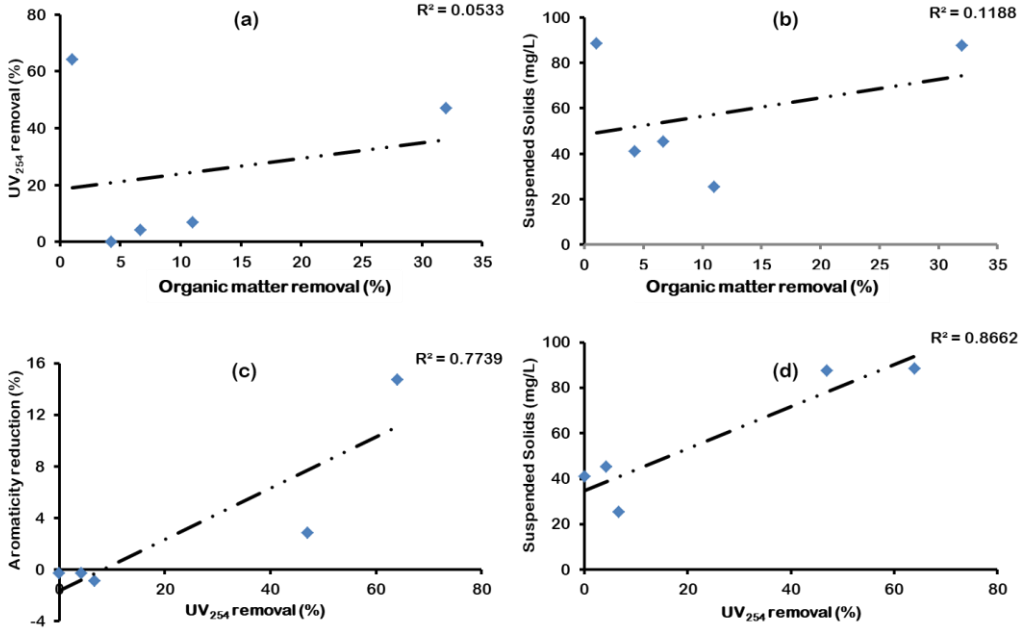

Fig. 1. Correlation of bulk parameters (a) correlation of UV_{254} removal with organic matter, (b) correlation of suspended solids with organic matter, (c) correlation of aromaticity reduction with UV_{254} removal and (d) correlation of suspended solids and UV_{254} removal.

There were wavelength shifts observed in the maximum fluorescence position of some peaks after 0.45 µm filtration. For example the excitation peak M for MV is red shifted (290 nm → 304 nm) nm, also red shifts were observed for the emission wavelengths for peak C for source waters PL (434 nm → 456 nm) and OL (438 nm → 442 nm). A blue shift was observed for the emission wavelength of peak M for the HL source (420 nm → 410 nm). Fluorescence quenching and inner filter effects collectively known as matrix effect affect the fluorescence signal [51]. The shifts were due to the removal of particulate matter which either masked or quenched the fluorescence of constituting flurophores. The potential reason for red or blue shifting after 0.45 µm filtering could be the transformation or change in composition or configuration of fluorescent organic matter fractions, e.g., the variation of the aromatic matter (in term of $SUVA_{254}$) [52]. The red shift is due to availability of alkoxyl containing substances, hydroxyl, carbonyl, carboxyl constituents and amino groups, while a blue shift is concomitant with the cleavage of larger molecules into smaller molecules or the disintegration of condensed aromatic functional groups [52].

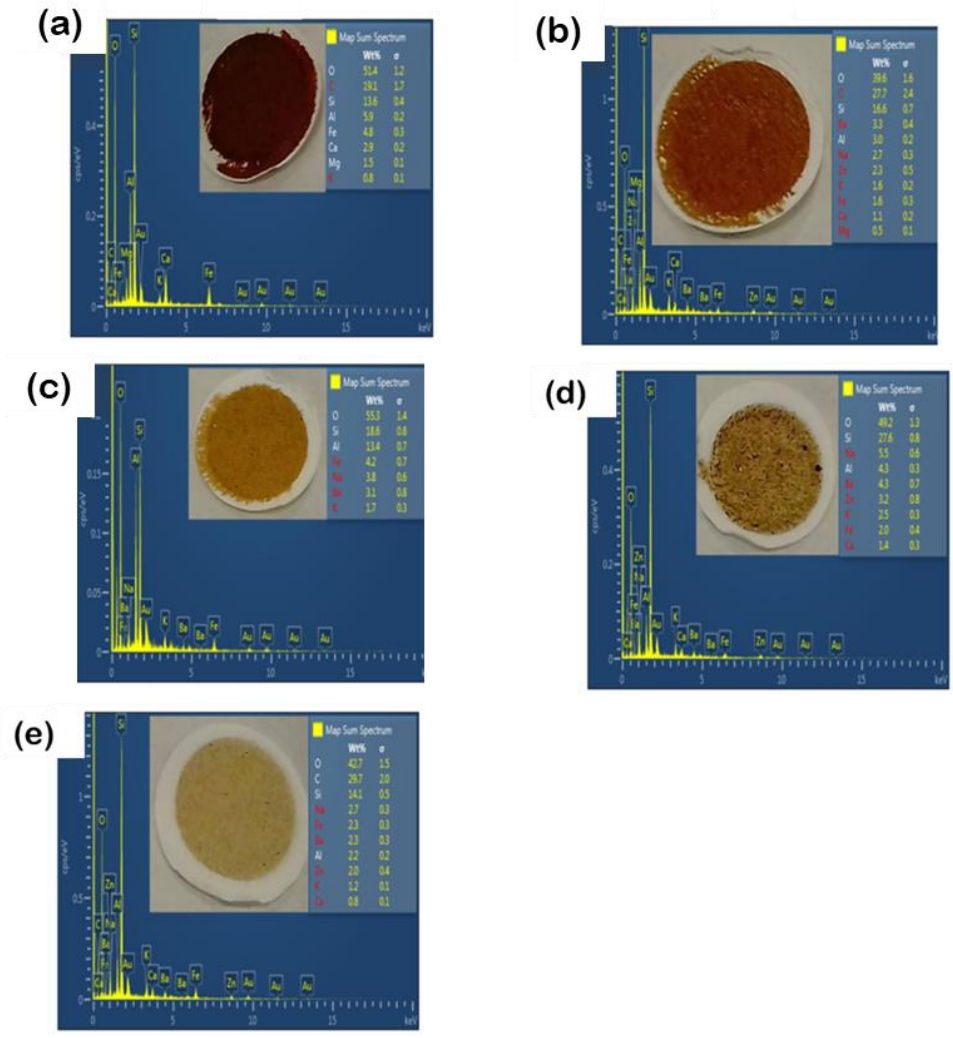

Fig. 2. Composition and distribution of inorganic particles after filtering 25 L of sample through a 0.45µm GF/F filter: (a) OL; (b) H; (c) P; (d) HL; and (e) MV.

3.1.4. The correlation of fluorescent organic matter composition and suspended solids

The identities of components were assigned to those in the database if similarity scores were greater than 0.97. Embedded visual pictorials and loading plots of the components are shown in Fig. 4 and Fig. A7, respectively. Component 1 (C1) was ascribed to humic like matter of terrestrial origin [53]. Spectral features of component 2 (C2) were catagorised as soil-derived fulvic acid-like matter [54], and component 3 (C3) was previously ascribed to humic-like, aromatic, conjugated macromolecular substances of terrestrial origin [55,56].

Suspended solids exhibited strong correlations with fluorescent fractions (R^2 = 0.82; 0.81 and 0.74 for C1; C2 and C3 respectively) (Fig. 4). Tian et al., (2013a) [13] observed a good correlation (R^2 = 0.79) between SS and particle fouling resistance using samples from a lake. Therefore it can be assumed that the extent of fouling is due to the synergy of the organic substrate and the particulate matter in water. It can then be concluded that particles are pivotal in the combined fouling layer formation with fluorescent organic matter even though particles by themselves may not be directly accountable to membrane fouling [58].

3.2. Interplay of particles, POM and DOM on fouling development and mechanism

3.2.1. Fouling resistance development during filtration

Thus far, we have demonstrated fundamental differences between POM and DOM found in different surface waters in South Africa. It is these differences that are hypothesized to cause variations in fouling behavior on ceramic membranes. The fouling development of total organic matter of source waters from H and PL mirrored each other (Fig. 5a). The organic matter and SS content was high for these coastal plants (22.67 mg/L.C:87.6 mg/L (SS); 19.58 mg/L.C:45.2 mg/L (SS) for H and PL, respectively). The fouling behavior for water samples from OL was expected to be just as high as the coastal plants because it had a high SS load (88.4 mg/L). However, this was not the case because of its low organic matter content (8.91mg/L.C). These results suggest a synergistic relationship exists between particles and organic matter in relation to fouling resistance development. The morphology of the resulting fouling layer contributes to the extent of permeate flux loss, inorganic foulants (SS) result in a loose static permeable layer, leading to low-concentration polarization and hindered back diffusion [42,59]. In contrast, organic foulants usually develop to a uniformly compressible permeate resistant layer that adheres to the active layer of the membrane [60]. So, depending on the proportion of the two in the water, the fouling layer will go towards a certain morphology. A comparison of the fouling resistance under different SS concentrations reported similar findings [13]. The hindered back diffusion of foulants in the combined layer was due to the synergistic impact of inorganic compounds and organic particles [61]. The consequence of synergistic fouling results in increased solution viscosity (concentration polarization) due to the accumulated organics on the active layer of the membrane consequently reducing the back transport of particles while the back diffusion of organics could be reduced by the accumulated particles on the ceramic active layer of the membrane [50].

The similarity of fouling development trend for all water sources, save for PL after removal of particles further supports synergistic fouling of particles and organic matter in fouling development (Fig. 5b). This uniformity can be attributed to membrane characteristics. The water contact angles (59.5°) demonstrated that the active layer of the membrane exhibited a hydrophilic surface (Fig. A4). This was further corroborated by the surface free energy components whose acid-base element was greater than 5 mJ/m^2.

Surface roughness values of 63 and 71 nm were recorded for randomly selected membranes (Fig. A5); this is an indication of a relatively smooth surface, which is ideal for a filtration process because it limits foulant/pollutant adhesion on the active layer of the membrane and subsequently enhances the anti-fouling characteristics of the membrane [42]. Even though the different waters were filtered through membranes with similar characteristics, the fouling development rate for water samples from PL was higher than the rest of the 0.45 µm filtered samples (Fig. 5b). This was attributed to its low conductivity (175µS.m^{-1}), which was the least compared to the rest of the 0.45 µm filtered samples. There was a linear relationship between electrical conductivity (*EC*) and ionic strength (*I*) [62].

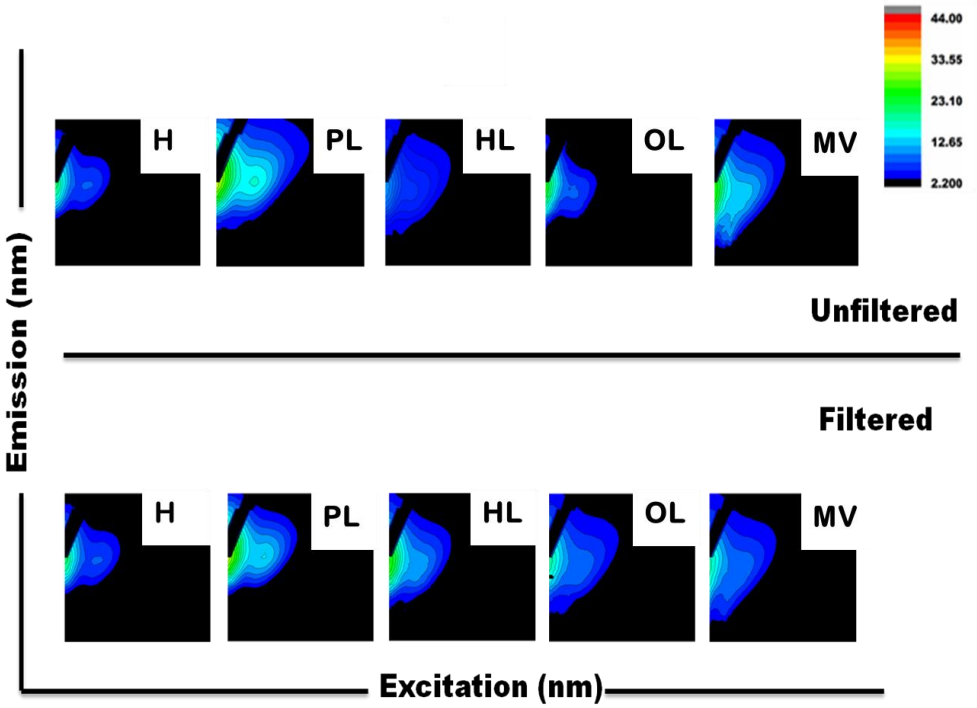

Fig. 3. Top panel shows EEMs for unfiltered water samples while the bottom panel shows EEMs for 0.45 µm filtered water samples.

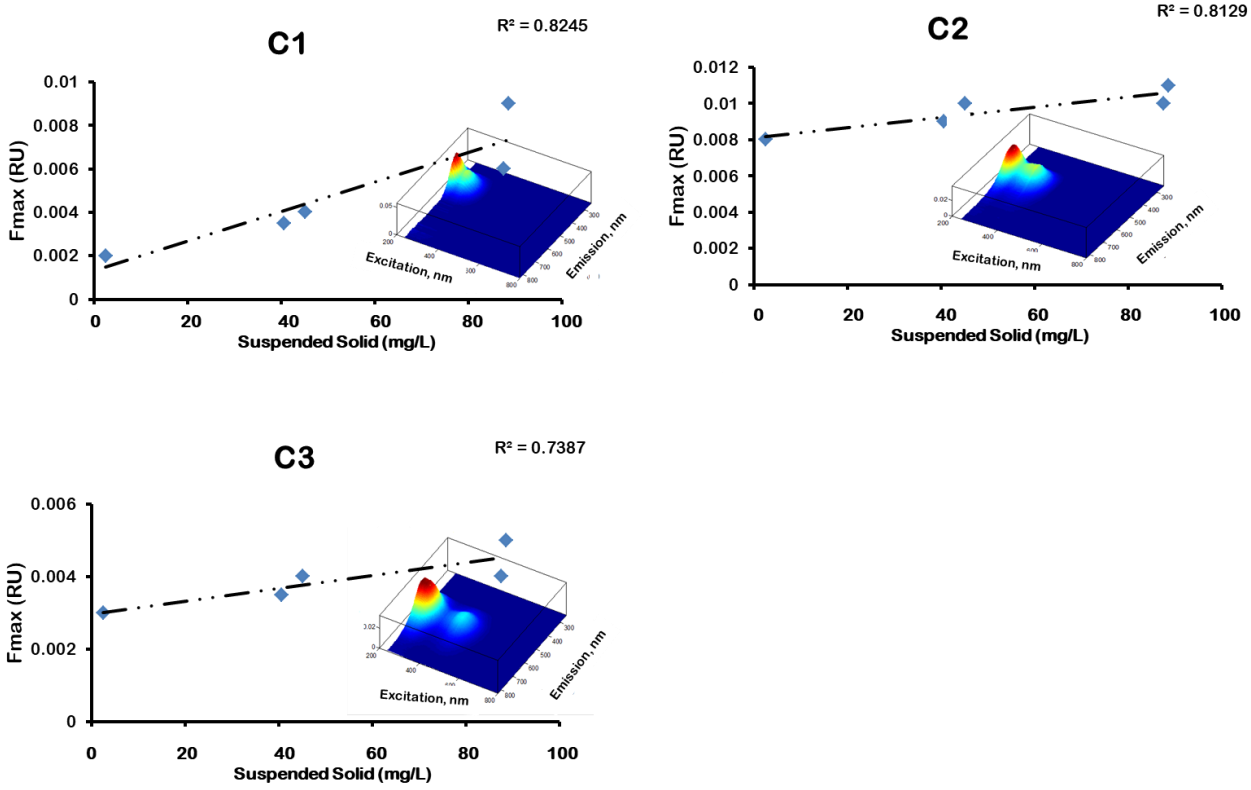

Fig. 4. Correlation of suspended solids with *PARAFAC* components. Visual pictorials of *PARAFAC* components are embedded.

Table 2
Difference in peak intensity and location following filtration through a 0.45 µm filter.

	Peak intensity (RU) and location - Ex (nm); Em (nm)				
	A	B	C	T	M
H unfiltered	17.5(260;448)	2.0(275;310)	8.6(350;448)	3.7(275;340)	8.9(310;420)
0.45 µm filtered	15.7(260;448)	0.7(275;310)	7.8(350;452)	2.0(275;340)	8.6(310; 420)
PL unfiltered	14.9(260;460)	0.6(275;310)	8.1(350;434)	1.3(275;340)	7.2(310;420)
0.45 µm filtered	14.0(260;460)	0.4(275;310)	7.6(350;456)	1.2(275;340)	6.9(310;420)
HL unfiltered	8.0 (260; 442)	2.0(275;310)	3.5(350;442)	2.8(275;340)	5.7(290;420)
0.45 µm filtered	7.8 (260; 442)	0.5(275;310)	3.3(350;442)	1.6(275;340)	4.5(304;410)
OL unfiltered	9.3 (260; 442)	2.1(275;310)	4.4(350;438)	2.9(275;340)	5.6(308;416)
0.45 µm filtered	7.3 (260; 442)	0.6(275;310)	3.4(350;442)	1.7(275;340)	4.2(310;416)
MV unfiltered	15.7(260;438)	6.2(275;310)	6.6(350;438)	7.7(275;340)	8.3(290;410)
0.45 µm filtered	13.5(260;438)	4.9(275;310)	6.4(350;438)	6.6(275;340)	8.5(302;410)

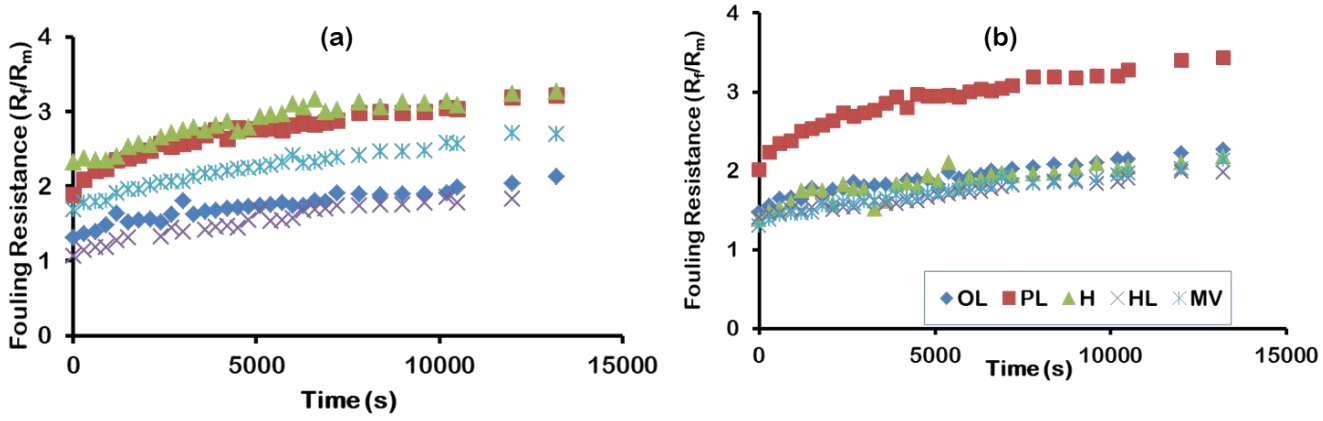

Fig. 5. Fouling resistance development due to (a) total fouling, and (b) organic fouling.

Ionic strength of the water determines the morphology of NOM; at low ionic strength NOM assumes a quasi-linear morphology [63]. The linear form of NOM fouls membranes more than the rigid form. Thus, as the experiment progressed layers upon layers deposit and compacted on the active layer of the membrane consequently increasing the rate of fouling with time.

The fouling development due to particles acting in tandem with organic matter and that of 0.45 µm filtered samples has been described. Further, the impact of solute characteristics has been shown to have an influence on the fouling development.

3.2.2. Irreversibility of membrane fouling by NOM fractions in the presence of particles and after pre-filtering with 0.45 µm filter

Source waters from OL, MV and PL exhibited higher organic irreversible fouling compared to total irreversible fouling (1.78:1.65; 1.60:1.33 and 1.58:1.06, respectively) (Fig. 6). While source waters from H and HL showed higher total irreversible fouling compared to organic fouling (2.84:1.83 and 1.86:1.74, respectively) (Fig. 6). The lower total irreversible fouling for OL, MV and PL was ascribed to the deposition of particles on the active layer of the membrane which consequently reduced the cake layer porosity. Prior research indicate the coefficient of hindered back diffusion depends on the membrane thickness and the porosity of the particle cake layer deposited on the active layer of the membrane [18, 22, 64]. An assessment of the severity of irreversible fouling between humic acid and humic acid spiked with particles of varying sizes found that the concentration and size of the micro particles did not have a significant effect on the irreversible fouling due to humic acid, which was due to the adsorption of humic acid molecules in the pores of the membrane [13]. The high total irreversible fouling for H and HL could be due to particles less than the MWCO of the membrane (450 Da) depositing inside the pores of the membranes. This finding highlighted the likelihood of the deposition of nanoparticles inside the membrane, constricting the pore sizes, consequently resulting in higher total irreversible fouling resistance.

Solute characteristics had a bearing on the severity of fouling. This phenomenon was exhibited by H and PL which showed higher irreversible fouling resistances in the total and organic fouling categories, respectively. As discussed in the previous section, the low ionic strength of source waters from PL conferred NOM with a quasi-linear morphology, which form compacted cake layers with smaller NOM fractions trapped even further in the membrane pores thus increasing the organic irreversible fouling [63]. Source waters from H had almost three-fold higher organic matter content compared to HL (22.67 and 8.28 mg/L.C, respectively). Furthermore, the peaks A, C and M were almost double than that of HL (17.5:9.3; 8.6:4.4 and 8.9:5.6 RU, respectively), regardless of almost similar concentrations of peak B and peak T (2.0:2.0 and 3.7:2.8 RU, respectively). Previous studies have shown humic-like matter to cause more severe irreversible fouling than the protein like fractions [65]. Additionally, the suspended solids content of H was almost four times that of HL (87.6 mg/L: 25.2 mg/L, respectively). As expected from these results, the severity of total irreversible fouling of H was at least double than that of HL, which turned out to be the case (Fig. 6).

3.2.3. Influence of feed water characteristics on fouling mechanisms

Fouling mechanisms of the feed waters was investigated by fitting the experimental results into the four classic filtration models (Fig. 7). The graphs were generated relative to time, and a linear segment of the graph denotes different mechanisms, namely cake filtration, intermediate blocking, standard blocking and complete blocking (Box A1), [20]. The R^2 value between time and specific linear flux segments determines the viability of the main fouling mechanism [20]. The summary of regression results of the membranes is presented in Table A2. For all raw water sources, R^2>0.9 (OL = 0.93, PL = 0.92, H = 0.95, HL = 0.90 and MV = 0.94), suggesting that fouling was a result of total irreversible fouling, the effect of which was greater for sources waters from H (R^2 = 0.95). This corroborates the findings where H exhibited the highest total irreversible fouling value (2.84 m^{-1}). The possible deposition

of nanoparticles inside the membranes, and the internal synergistic fouling with the incoming organic matter could have facilitated standard fouling to be the preferred fouling mechanism leading to total irreversible fouling from all raw source waters [12]. The alternative explanation stems from the S_R values; higher and lower S_R values denote lower and higher molecular weight organic matter [37]. The S_R values of source waters from OL, MV, HL, H and PL were 2.27, 1.4, 1.23, 0.92 and 0.85, respectively. This implies OL had organic matter of least molecular weight in relative terms, and such could deposit deeper in the pores of the membranes, even in narrow pores, thus supporting standard fouling mechanism. The mechanism of the standard blocking results in the constriction of the internal pores of the membranes due to the continual deposition of smaller contaminants consequently leading to irreversible fouling [66]. Possibly, larger particles were continually deposited onto the active layer of the membrane as time progressed, either completely blocking the membrane pores or acting as nucleation sites for attachment of organic matter. This assumption is supported by R^2 for complete blocking which was also above 0.9 for all raw water sources (OL = 0.94, PL = 0.93, H = 0.95, HL = 0.95 and MV = 0.92). Although this form of fouling is reversible, the results show the presence of particles enhances this mechanism of fouling. Cake filtration was the least favored fouling mechanism with $R^2 \leq 0.8$ (OL = 0.79, PL = 0.8, H = 0.80, HL = 0.52 and MV = 0.61). The presence of particles on the active layer of the membrane created a porous or spongy layer which offered less resistance to back diffusion, thus cake filtration was the least favored fouling mechanism in the presence of inorganic particles.

The removal of inorganic particles shifted the fouling mechanisms as indicated by the regression coefficients (Table A2). The most favored fouling mechanism was cake filtration (OL = 0.97, PL = 0.75, H = 0.76, HL = 0.71 and MV = 0.76). The removal of particles might have resulted in a more compacted cake layer. Notably, complete and standard blocking were the favored fouling mechanisms for OL, PL and MV (complete: 0.79, 0.95 and 0.91, respectively; standard: 0.81, 0.95 and 0.91, respectively). The membranes used were in the nanofiltration range and prior researched has shown that complete blocking is the likely fouling mechanism due to the deposition of smaller contaminants at the mouth of membrane [30,66]. The removal of particles enhanced the compaction of the cake layer, subsequently increasing the rate of complete pore blocking and enhancing standard blocking by smaller organic matter in the interior of the membrane. Source waters from PL were more inclined to these types of fouling after removal of particles, thus elevated organic irreversible fouling resistance was mainly due to interplay of complete (R^2 = 0.95) and standard (R^2 = 0.95) blocking, corroborating our earlier findings. As discussed in previous sections, the physico-chemical parameters of PL source water inferred a quasi-linear morphology of the organic matter. This was further supported by the least S_R (0.84) value, implying a relatively larger molecular weight. Therefore this meant the compaction of the cake layer was by larger molecular weight organic matter, implicating cake filtration to play a dominant role in fouling by 0.45 µm pre-filtered waters from PL. The mechanism of cake filtration involves large particles adsorbing and depositing on the surface of the membrane, consequently causing the formation of a cake layer [60,66].

It must be noted that size exclusion cannot solely be attributed to the rejection mechanism because no one membrane could exclusively and entirely remove NOM and its fractions. Rejection is a function of interplay between the physicochemical properties of the foulant and the foulant-membrane interactions [67].

3.2.4. Influence of feed chemistry and membrane characteristics on the cake layer development

In the past fouling models were mainly used to describe fouling on polymeric membranes [63], the linear fit of these mathematical models based on cake filtration can well describe ceramic membrane fouling by NOM fractions in the treatment of surface water. MFI was determined by graphing t/V against cumulative filtrate volume, V (Fig. 8; Table 3). In the determination of MFI for nanofiltration membranes, the main fouling mechanism is attributed to cake filtration [68].

The MFI value for raw unfiltered PL sample (34 582 s/L^2) was more than ten times greater than that of MV 2 699 s/L^2, regardless of almost similar SS and organic matter content (45.2 mg/L : 19.58 mg/L.C and 40.8 mg/L : 17.63 mg/L.C, respectively). The build up to cake filtration was more likely for raw PL water (R^2 = 0.8) compared to MV (R^2 = 0.61), although the two water sources had comparable SS content (45.2 mg/L and 40.8 mg/L for PL and MV, respectively). Probably the particles sizes in MV source water were larger than those in PL source water. Cross filtration hydrodynamics such as back diffusive forces (shear, inertia lift effects and cross flow velocity) prevent the over deposition of large particles on the active layer of the membrane [69,70]. Consequently, cross flow reduces concentration polarization and consequently the effect of fouling considerably due to the influence of cross flow hydrodynamics [30,50]. Further, the deposition of larger particles on the membrane active layer leads to the development of a porous or spongy layer which offers less resistance to back diffusion. Thus cake filtration was the least likely fouling mechanism for MV compared to PL in the presence of inorganic particles.

Water samples from H and OL had similar concentrations of SS (87.6 mg/L and 88.4 mg/L, respectively) and MFI values for raw samples (6625 and 8060 s/L^2, respectively), despite a very large difference in organic matter quantity (22.67 mg/L.C and 9.81 mg/L.C). This can be explained by organic matter adsorbing onto the surface of particles which could have deposited on the active layer of the membrane and nanoparticles in the interior of the membranes, and consequently, the deposition of NOM fractions in the pores of membrane and/or the active layer of the membrane was considerably reduced. A previous study reported that when particles and organics are combined the fouling indices were always less than those obtained from experiments of organics and particles separately [22].

The MFI value for raw OL sample was 8060 s/L^2, doubling that of HL (4005 s/L^2) despite similar organic matter quantity (8.91 mg/L.C and 8.28 mg/L.C, respectively). The S_R value for OL was 2.27 while that for HL was 1.23, implying the molecular size of organic matter for HL was almost double that in OL. In cross flow systems, the cross-flow sheer forces larger organic matter particles to recirculated with the retentate, and the deposited cake layer formed is mainly formed by smaller organic matter particles [22]. Moreover, larger particles occupy larger surface area on the active layer of the membrane compared to smaller particles, furthermore, small enough particles can even pass through the pore mouth of the membrane and deposit deeper in the interior of the membrane.

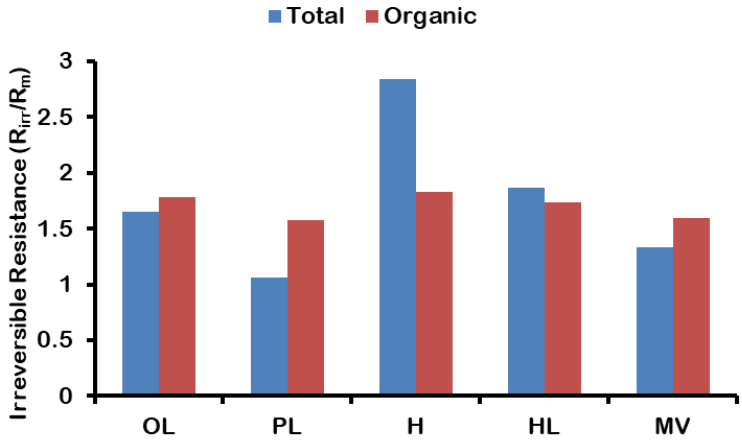

Fig. 6. Irreversibility of membrane fouling by NOM in the presence of particles (total) and after pre-filtering through 0.45 µm filter (organic).

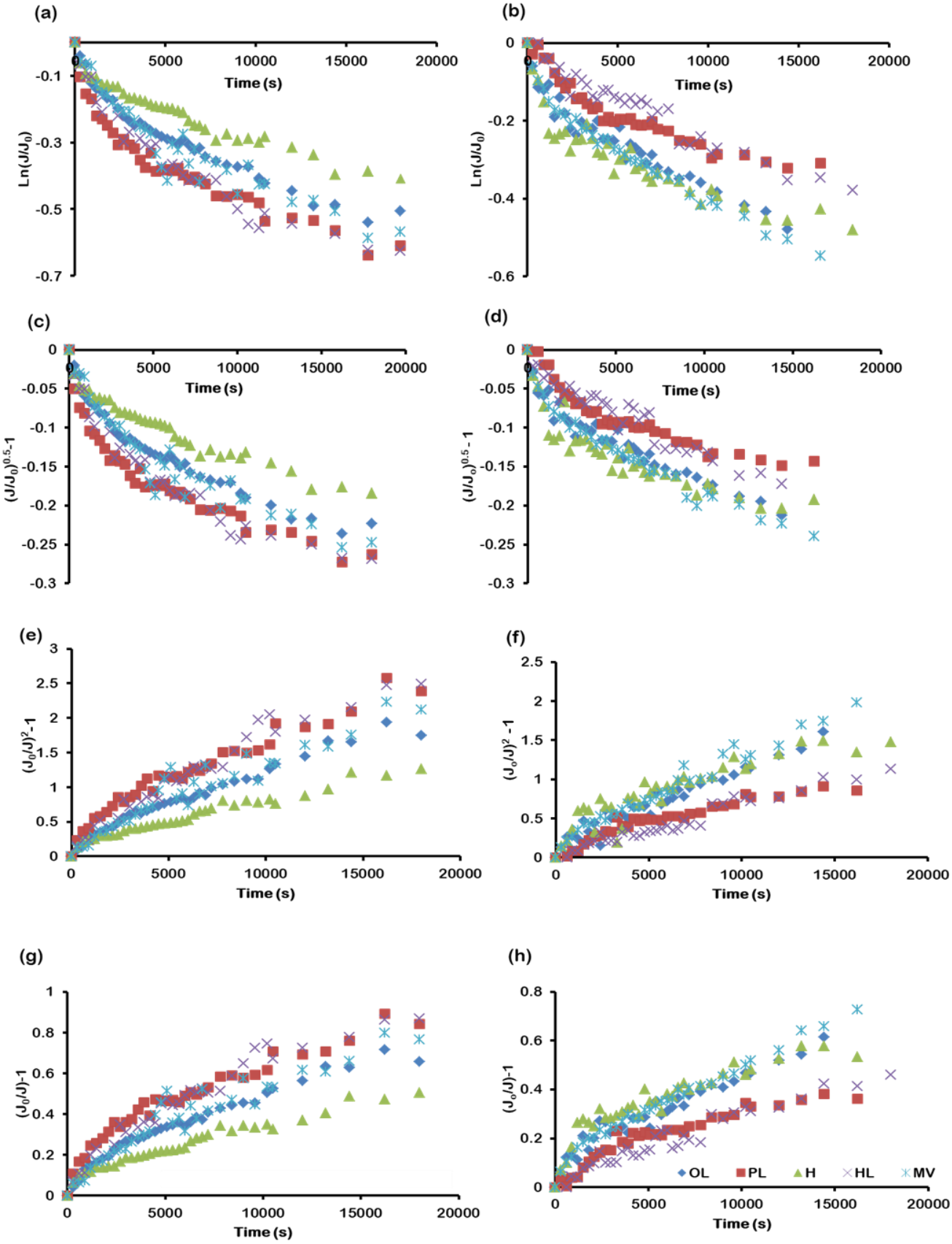

Fig. 7. Linear expressions modeling mechanism of complete blocking: (a) raw unfiltered samples, (b) 0.45 µm prefiltered samples; Standard blocking: (c) raw unfiltered samples, (d) 0.45 µm prefiltered samples; cake filtration: (e) raw unfiltered samples, (f) 0.45 µm prefiltered samples and; intermediate blocking: (g) raw unfiltered samples, (h) 0.45 µm prefiltered samples

The removal of particulate matter reduced the synergistic fouling leading to cake layer development to different extents: H-78%; PL-69%; HL-40%; OL-16% and MV-25% (Table 3). The dominant factors in cake layer development after filtering through 0.45 µm were due to DOM characteristics and foulant-membrane interactions. Notably, the MFI value for OL was higher than for HL (6 739 and 2 394 s/L^2, respectively) despite comparable aromaticity (11 and 12 %, respectively), and peak C intensity values (4.4 and 3.5 RU, respectively). This could be because peak C is made up of fulvic acid-like and humic acid-like groups [71]**.** Humic acids (HAs) are bulky molecules containing aromatic functional groups, they also contain polar groups such as phenolic and carboxylic moieties [23]. Fulvic acids (FAs) are usually smaller in molecular size, and contain less aromatic functional groups, however, they contain relatively more phenolic and carboxylic moieties [23]. The low S_R value for HL (1.23) compared to OL (2.27) indicate HL to be composed of larger molecular weight organic matter fractions typically HAs. It is the extent of polar interactions with the hydroxyl groups inherent in ceramic membranes that leads to severity of fouling [17]. Because of the bulkiness of the HA, there are steric hindered polar interactions between the hydroxyl and the carboxylic and phenolic groups of HAs, thus leading to less severity of cake layer development compared to FA which is less bulky [23]. MFI is inversely proportional to the *TMP* applied and directly proportional to the fouling potential of the feed stream water, thus MFI can act as a comparison proxy for fouling potential of different feed waters.

The results demonstrate the interplay of foulant physico-chemistry, foulant-foulant, and membrane-foulants interactions. In this case, the foulant is organic matter from different sources with different physico-chemical characteristics and the other foulant is the inorganic particles found *in situ*.

4. Conclusions

This study demonstrated the extent of the background electrolytes, foulant concentration, foulant-membrane, foulant-foulant interactions and foulant type (physicochemical properties) of feed water on the fouling development and mechanism on ceramic membranes. Robust characterization of the feed waters was conducted and the key findings were:

(1) When the results where pooled together, a strong correlation was found between UV_{254} removal and suspended solids (R^2 = 0.87), showing that UV_{254} absorbing groups had a preferential adsorption affinity to inorganic particles.
(2) Suspended solids exhibited strong correlations with fluorescent fractions (R^2 = 0.82; 0.81 and 0.74 for C1; C2 and C3, respectively), thus confirming synergistic association between particles and fluorescent organic components in the fouling of ceramic membranes.
(3) Even though the different source waters were filtered through ceramic membranes with similar characteristics, the fouling development rate for PL was higher than the rest of the 0.45 µm pre-filtered samples. This was attributed to its low conductivity, translating to a quasi-linear morphology in low ionic strength environment.
(4) Inorganic particles act as nucleating agents with the organic components adsorbing on its surface during fouling layer formation resulting in heavier aggregates that deposit easily and adhere poorly. This was observed with source waters from H and OL had similar suspended solids and MFI values, despite a very large difference in organic matter quantity. Organic matter adsorbed onto the surface of particles which deposited on the active layer of the membrane and nanoparticles in the interior of the membranes. Consequently, NOM deposition inside the pores of the membranes or the active layer of the membrane reduced significantly.

Future research should focus on: (1) investigating the relationship between pore size distribution and MWCO during the rejection of unfiltered and 0.45 µm pre-filtered samples, (2) determine the particle size and organic matter fraction distribution (LC-OCD fractions) of unfiltered and 0.45 µm pre-filtered samples, (3) investigating the relationship between membrane charge and the rejection mechanism of unfiltered and 0.45µm pre-filtered samples, and (4) investigating the impact of other contaminants such as oil, TSS and COD on the fouling behaviors of unfiltered and 0.45 µm pre-filtered samples.

Acknowledgements

Special acknowledgements to Technical University of Delft (TU Delft) for providing training on membrane technology and providing the ceramic membranes. The authors are also grateful for funding from the Water Research Commission (WRC) of South Africa; the National Research Foundation (NRF), South Africa; and the University of South Africa (UNISA).

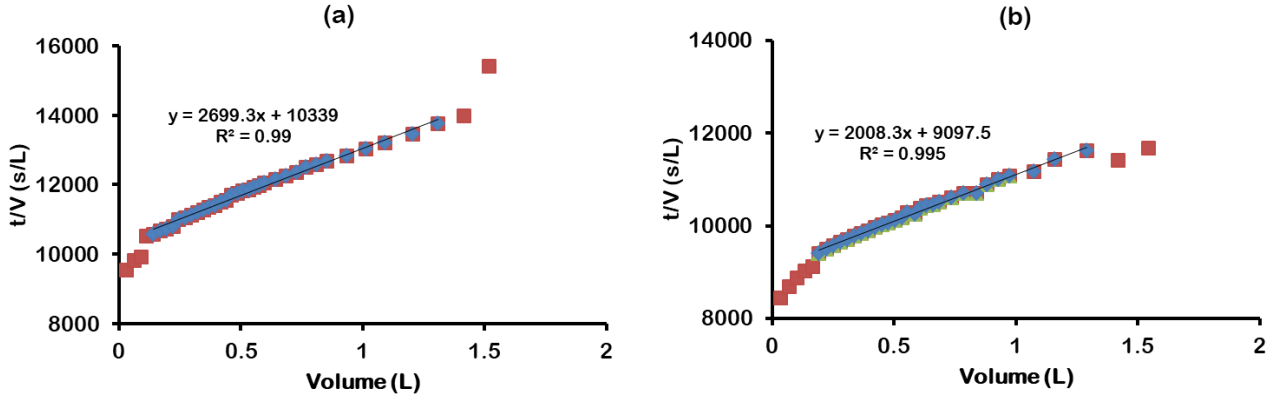

Fig. 8. Determination of MFI for (a) unfiltered, and (b) 0.45 µm filtered samples using best-fit regression lines.

Table 3
Summary of MFI values and their goodness of fit for unfiltered and 0.45 pre-filtered water samples.

	OL	PL	H	HL	MV
MFI (s/L^2)					
unfiltered	8060.3	34582	6625.7	4005.3	2699.3
0.45 Filtered	6739.1	10611	1461.4	2394.9	2008.3
R^2					
Unfiltered	0.97	0.98	0.99	0.97	0.99
0.45 filtered	0.98	0.98	0.97	0.99	1

References

[1] A. Matilainen, N. Lindqvist, S. Korhonen, T. Tuhkanen. Removal of NOM in the different stages of the water treatment process. Environ. Int.28 (6), 457–465, 2003. DOI: 10.1016/S0160-4120(02)00071-5

[2] K. P. Lobanga. Natural organic matter removal from surface waters by enhanced coagulation, granular activated carbon adsorption and ion exchange. PhD Thesis, University of Johannesburg, 2012.

[3] T. I. Nkambule. Natural Organic Matter (Nom) in South African Waters: Characterization of Nom, Treatability and Method Development for Effective Nom Removal From Water. PhD Thesis, University of Johannesburg, 2012.

[4] P. Krzeminski, C. Vogelsang, T. Meyn, S.J Kohler, H. Poutanen, H.A de Wit, W. Uhl. Natural organic matter fractions and their removal in full-scale drinking water treatment under cold climate conditions in Nordic capitals. J. Environ. Manage, 241 (2018) 427–438. https://doi.org/10.1016/j.jenvman.2019.02.024

[5] E. Vasyukova, R. Proft, J. Jousten, I. Slavik, W. Uhl. Removal of natural organic matter and trihalomethane formation potential in a full-scale drinking water treatment plant. Water Sci. Technol. Water Supply 13 (4) 1099, 2013.

[6] P. Tshindane, P.P. Mamba, L. Moss, U.U. Swana, W. Moyo, M.M. Motsa, N. Chaukura, B.B. Mamba,T.I.T. Nkambule.The occurrence of natural organic matter in South African water treatment plants. J. Water Process Eng 31 (2019) 100809. https://doi.org/10.1016/j.jwpe.2019.100809

[7] L. Lin, X. Xu, C. Papelis, P. Xu. Innovative use of drinking water treatment solids for heavy metals removal from desalination concentrate: Synergistic effect of salts and natural organic matter. Chem. Eng. Res. Des 120 (2017) 231–239. https://doi.org/10.1016/j.cherd.2017.02.009

[8] U. M. Aliyu, S. Rathilal, Y. M. Isa. Membrane desalination technologies in water treatment: A review. Water Pract. Technol 13 (4) 738–752, 2018. DOI: 10.2166/wpt.2018.084

[9] G. Kastl, A. Sathasivan, I. Fisher. A selection framework for NOM removal process for drinking water treatment. Desalin. Water Treat 3994 (December), 1–11, 2016. https://doi.org/10.1080/19443994.2015.1044476

[10] A. W. Zularisam, A. F. Ismail, M. R. Salim, M. Sakinah, H. Ozaki. The effects of natural organic matter (NOM) fractions on fouling characteristics and flux recovery of ultrafiltration membranes. Desalination 212 (1–3) 191–208, 2007. https://doi.org/10.1016/j.desal.2006.10.010

[11] A. M. Hansen, T. E. C. Kraus, B. A. Pellerin, J. A. Fleck, B. D. Downing, B. A. Bergamaschi. Optical properties of dissolved organic matter (DOM): Effects of biological and photolytic degradation. Limnol. Oceanogr 61 (3) 1015–1032, 2016. https://doi.org/10.1002/lno.10270

[12] M.D. Yu, X.S. He, B.D Xi, R.T. Gao, X.W. Zhao, H. Zhang, H. Zhang, C.H. Huang, W. Tan. Investigating the composition characteristics of dissolved and particulate/colloidal organic matter in effluent-dominated stream using fluorescence spectroscopy combined with multivariable analysis. Environ. Sci. Pollut. Res 25 (9) 9132–9144, 2018. DOI: 10.1007/s11356-018-1190-4

[13] J. Tian, M. Ernst, F. Cui, M. Jekel. Effect of different cations on UF membrane fouling by NOM fractions. Chem. Eng. J 223 (2013) 547–555. https://doi.org/10.1016/j.cej.2013.03.043

[14] T. O. Mahlangu, J. M. Thwala, B. B. Mamba, A. D'Haese, A. R. D. Verliefde. Factors governing combined fouling by organic and colloidal foulants in cross-flow nanofiltration. J. Membr. Sci 491 (July) 53–62, 2015. https://doi.org/10.1016/j.memsci.2015.03.021

[15] M. Schulz, A. Soltani, X. Zheng, M. Ernst. Effect of inorganic colloidal water constituents on combined low-pressure membrane fouling with natural organic matter (NOM). J. Membr. Sci 507 (2016) 154-164. https://doi.org/10.1016/j.memsci.2016.02.008

[16] D. Li, D.I. Kaplan, H.S. Chang, J.C. Seaman, P.R. Jaffe, P.K van Groos, K.G. Scheckel, C.U. Segre, N. Chen, D.T. Jiang, M. Newville, A. Lanzirotti. Spectroscopic evidence of uranium immobilization in acidic wetlands by natural organic matter and plant roots. Environ. Sci. Technol 49 (5) 2823–2832, 2015. https://doi.org/10.1021/es505369g

[17] S. Metsämuuronen, M. Sillanpää, A. Bhatnagar, M. Mänttäri. Natural Organic Matter Removal from Drinking Water by Membrane Technology. Sep. Purif. Technol 43 (July) 1–61, 2014. https://doi.org/10.1080/15422119.2012.712080

[18] D. Jermann, W. Pronk, R. Kägi, M. Halbeisen, M. Boller. Influence of interactions between NOM and particles on UF fouling mechanisms. Water Res 42 (14) 3870–3878, 2008. https://doi.org/10.1016/j.watres.2008.05.013

[19] J. yu Tian, M. Ernst, F. Cui, M. Jekel. Effect of particle size and concentration on the synergistic UF membrane fouling by particles and NOM fractions. J. Membr. Sci, 446 (2013) 1–9. https://doi.org/10.1016/j.memsci.2013.06.016

[20] L. De Angelis, M. Marta, F. De Cortalezzi. Ceramic membrane filtration of organic compounds : Effect of concentration , pH , and mixtures interactions on fouling. Sep. Purif. Technol 118 (2013) 762–775. DOI: 10.1016/j.seppur.2013.08.016

[21] T. Persson and M. Wedborg. Multivariate evaluation of the fluorescence of aquatic organic matter. Analytica Chimica Acta 434 (2001) 179–192. https://doi.org/10.1016/S0003-2670(01)00812-1

[22] M. H. Le, K. J. Kim, A. Jang. Foulant–foulant Interaction of Combined Micro-particulate and Organic Fouling on a Ceramic Membrane. KSCE J. Civ. Eng 22 (12) 4814–4825, 2018. https://doi.org/10.1007/s12205-018-0611-8

[23] G. Mustafa, K. Wyns, A. Buekenhoudt, V. Meynen. Antifouling grafting of ceramic membranes validated in a variety of challenging wastewaters. Water Res 104 (2016) 242–253. DOI: 10.1016/j.watres.2016.07.057

[24] L. M. Corneal, S. J. Masten, S. H. R. Davies, V. V Tarabara, S. Byun, M. J. Baumann. AFM , SEM and EDS characterization of manganese oxide coated ceramic water filtration membranes. J. Membr. Sci 360 (1–2) 292–302, 2010. https://doi.org/10.1016/j.memsci.2010.05.026

[25] M. M. Pendergast E. M. V. Hoek. A review of water treatment membrane nanotechnologies. Energy Environ. Sci 4 (6) 1946, 2011. https://doi.org/10.1039/C0EE00541J

[26] T. Meyn. NOM Removal in Drinking Water Treatment Using Dead-End Ceramic Microfiltration. Ph.D Thesis, Norwegian University of Science and Technology, 2011.

[27] F. Chen et al. Pilot-scale investigation of drinking water ultrafiltration membrane fouling rates using advanced data analysis techniques. Water Res 48 (2013) 508–518. https://doi.org/10.1016/j.watres.2013.10.007

[28] H. Yamamura, K. Okimoto, K. Kimura, Y. Watanabe. Hydrophilic fraction of natural organic matter causing irreversible fouling of microfiltration and ultrafiltration membranes. Water Res 54 (2014) 123–136. https://doi.org/10.1016/j.watres.2014.01.024

[29] W. Yu, T. Liu, J. Crawshaw, T. Liu, N. Graham. Ultrafiltration and nanofiltration membrane fouling by natural organic matter: Mechanisms and mitigation by pre-ozonation and pH. Water Res 139 (2018) 353-362. https://doi.org/10.1016/j.watres.2018.04.025

[30] L. F. Fang, N.K. Kato, H.Y. Yang, L. Cheng, S. Hasegawa, S. Jeon, H. Matsuyama. Evaluating the Antifouling Properties of Poly(ether sulfone)/Sulfonated Poly(ether sulfone) Blend Membranes in a Full-Size Membrane Module. Ind. Eng. Chem. Res 57 (12) 4430–4441, 2018. https://doi.org/10.1021/acs.iecr.8b00114

[31] Z. Zhou, L. Guo. A critical evaluation of an asymmetrical flow field-flow fractionation system for colloidal size characterization of natural organic matter. J. Chromatogr. A 1399 (2015) 53–64. DOI: 10.1016/j.chroma.2015.04.035

[32] K. Kimura, Y. Oki. Efficient control of membrane fouling in MF by removal of biopolymers: Comparison of various pretreatments. Water Res 115 (2017) 172–179. DOI: 10.1016/j.watres.2017.02.033

[33] M. M. Motsa, B. B. Mamba, A. R. D. Verliefde. Forward osmosis membrane performance during simulated wastewater reclamation: Fouling mechanisms and fouling layer properties. J. Water Process Eng 23, no (2018) 109–118. https://doi.org/10.1016/j.jwpe.2018.03.007

[34] C. Khorshed, S. Vigneswaran, J. Kandasamy, R. Aryal, D. Dharmapalan. Assessment of water treatment processes : detailed organic matter characterisation and membrane fouling indices at the Loddon Water Treatment Plant , Victoria , Australia. Water Sci. Technol. Water Supply 11(3) 274–280, 2011. https://doi.org/10.2166/ws.2011.040

[35] K. Y. Jee, D. H. Shin, Y. T. Lee. Surface modification of polyamide RO membrane for improved fouling resistance. Desalination. 394 (2016) 131–137. https://doi.org/10.1016/j.desal.2016.05.013

[36] S. N. Ndiweni,M.C. Chys,N. Chaukura,S.W. H. van Hulle, T.T. I. Nkambule. Assessing the impact of environmental activities on natural organic matter in South Africa and Belgium. Environ. Tech. 40(13) 3330 (2019). https://doi.org/10.1080/09593330.2019.1575920

[37] J. R. Helms, A. Stubbins, J. D. Ritchie, E. C. Minor, D. J. Kieber, K. Mopper. Absorption spectral slopes and slope ratios as indicators of molecular weight, source, and photobleaching of chromophoric dissolved organic matter. Limnol. Oceanogr 53 (3) 955–969, 2008. https://doi.org/10.4319/lo.2008.53.3.0955

[38] Y. Zhang, Y. Zhou, K. Shi, B. Qin, X. Yao, Y. Zhang. Optical properties and composition changes in chromophoric dissolved organic matter along trophic gradients : Implications for monitoring and assessing lake eutrophication. Water Res 131 (2018) 255–263. https://doi.org/10.1016/j.watres.2017.12.051

[39] J. Xing, H. Liang, X. Cheng, H. Yang, D. Xu, Z. Gan, X. Luo, X. Zhu, G. Li. Combined effects of coagulation and adsorption on ultrafiltration membrane fouling control and subsequent disinfection in drinking water treatment Environ. Sci. Pollut. Res 26 (2019) 33770–33780. https://doi.org/10.1007/s11356-018-2416-1

[40] K. R. Murphy, C. A. Stedmon, D. Graeber, R. Bro. Fluorescence spectroscopy and multi-way techniques. PARAFAC. Anal. Methods 5 (23) 6557–6566, 2013. https://doi.org/10.1039/C3AY41160E

[41] K. R. Murphy, C. A. Stedmon, P. Wenig, R. Bro. Analytical Methods OpenFluor – an online spectral library of auto- fluorescence by organic compounds in the environment. Anal. Methods 6 (2014) 658–661. DOI: 10.1039/c3ay41935e

[42] M. M. Motsa, B. B. Mamba, A. R. D. Verliefde. Combined colloidal and organic fouling of FO membranes: The influence of foulant–foulant interactions and ionic strength. J. Membr. Sci 493 (July) 539–548. https://doi.org/10.1016/j.memsci.2015.06.035

[43] R. Shang, A. Goulas, C. Y. Tang, X. de Frias Serra, L. C. Rietveld, S. G. J. Heijman. Atmospheric pressure atomic layer deposition for tight ceramic nanofiltration membranes: Synthesis and application in water purification. J. Membr. Sci 528 (January) 163–170, 2017. https://doi.org/10.1016/j.memsci.2017.01.023

[44] C. H. Koo, A. W. Mohammad, F. Suja', M. Z. Meor Talib. Setting-up of modified fouling index (MFI) and crossflow sampler-modified fouling index (CFS-MFI) measurement devices for NF/RO fouling. J. Membr. Sci 435 (2013) 165–175. https://doi.org/10.1016/j.memsci.2013.02.027

[45] P. Li, J. Hur. Utilization of UV-Vis spectroscopy and related data analyses for dissolved organic matter (DOM) studies: A review. Crit. Rev. Environ. Sci. Technol 47 (3) 131–154, 2017. https://doi.org/10.1080/10643389.2017.1309186

[46] O. E. Trubetskaya, C. Richard, O. A. Trubetskoj. High amounts of free aromatic amino acids in the protein-like fluorescence of water-dissolved organic matter.

Environ. Chem. Lett 14 (2016) 495–500. DOI 10.1007/s10311-016-0556-4

[47] S. A. Baghoth. Characterizing natural organic matter in drinking water treatment proCesses and trains saeed abdallah baghoth. PhD Thesis, Technical University of Delft, 2012. ISBN 978-1-138-00026-1 (Taylor & Francis Group)

[48] T. Kikuchi, M. Fujii, K. Terao, R. Jiwei, Y. P. Lee, C. Yoshimura. Correlations between aromaticity of dissolved organic matter and trace metal concentrations in natural and ef fl uent waters : A case study in the Sagami River Basin , Japan. Science of the Total Environment 576 (2017) 36–45. https://doi.org/10.1016/j.scitotenv.2016.10.068

[49] Y. Zhang, X. Zhao, X. Zhang, S. Peng. A review of different drinking water treatments for natural organic matter removal. Water Sci. Technol. Water Supply 15 (3) 442, 2015. https://doi.org/10.2166/ws.2015.011

[50] M. M. Motsa, B. B. Mamba, A. D'Haese, E. M. V Hoek, A. R. D. Verliefde. Organic fouling in forward osmosis membranes: The role of feed solution chemistry and membrane structural properties. J. Membr. Sci 460 (July) 99–109, 2014. https://doi.org/10.1016/j.memsci.2014.02.035

[51] B. Dalmacija, J. Agbaba, J. Molnar, A. Tubic. Effects of water matrix and ozonation on natural organic matter fractionation and corresponding disinfection by-products formation. Water Sci. Technol. Water Supply 15 (1) 75–83, 2015. https://doi.org/10.2166/ws.2014.086

[52] H. Zhu, X. Wen, X. Huang. Characterization of membrane fouling in a micro fi ltration ceramic membrane system treating secondary effluent. Desalination 284 (2012) 324–331. https://doi.org/10.1016/j.desal.2011.09.019

[53] U. J. Wu, K. R. Murphy, C. A. Stedmon. The One-Sample PARAFAC Approach Reveals Molecular Size Distributions of Fluorescent Components in Dissolved Organic Matter. Environ. Sci. Technol 51 (20) 11900–11908, 2017. https://doi.org/10.1021/acs.est.7b03260

[54] C. L. Osburn, T. J. Boyd, M. T. Montgomery, T. S. Bianchi, R. B. Coffin, H. W. Paerl. Optical Proxies for Terrestrial Dissolved Organic Matter in Estuaries and Coastal Waters. Frontiers in Marine Science 2:127.doi: 10.3389/fmars.2015.00127

[55] K. M. Cawley. Characterising the sources and fate of dissolved organic matter in Shark Bay , Australia : a preliminary study using optical properties and stable carbon isotopes. Marine and Freshwater Research 63(11) 1098-1107, 2012. https://doi.org/10.1071/MF12028

[56] C. L. Osburn, L. T. Handsel, B. L. Peierls, H. W. Paerl. Predicting Sources of Dissolved Organic Nitrogen to an Estuary from an Agro-Urban Coastal Watershed. Environ. Sci. Technol 50 (16) 8473–8484, 2016. https://doi.org/10.1021/acs.est.6b00053

[57] J. yu Tian, M. Ernst, F. Cui, M. Jekel. Correlations of relevant membrane foulants with UF membrane fouling in different waters. Water Res 47 (3) 1218–1228, 2013. https://doi.org/10.1016/j.watres.2012.11.043

[58] R.H. Peirisa, C. Hallé, H. Budman, C. Moresoli, S. Peldszus, P. M.Huck, R.L. Legge.Identifying fouling events in a membrane-based drinking water treatment process using principal component analysis of fluorescence excitation-emission matrices. Water Res 44(2010) 185–194. https://doi.org/10.1016/j.watres.2009.09.036

[59] Y. Guo, Z. Song, B. Xu, Y. Li, F. Qi, J. Croue. A novel catalytic ceramic membrane fabricated with CuMn 2 O 4 particles for emerging UV absorbers degradation from aqueous and membrane fouling elimination. J. Hazard. Mater 344 (2018) 1229–1239. https://doi.org/10.1016/j.jhazmat.2017.11.044

[60] H. Wang, M. Park, H. Liang, S. Wu, I.J. Lopez, W. Ji, G. Li, S.A.Snyder. Reducing ultrafiltration membrane fouling during potable water reuse using pre-ozonation. Water Res 125 (2017) 42-51. http://dx.doi.org/10.1016/j.watres.2017.08.030 0

[61] Q. Li, M. Elimelech. Natural organic matter fouling and chemical cleaning of nanofiltration membranes. Water Sci. Technol. Water Supply 4(5-6)245–252, 2004. https://doi.org/10.2166/ws.2004.0114

[62] F. L. Rosario-Ortiz, S. Snyder, I. H. Suffet. Characterization of the polarity of natural organic matter under ambient conditions by the Polarity Rapid Assessment Method (PRAM). Environ. Sci. Technol. 41(14) 4895–4900, 2007. https://doi.org/10.1021/es062151t

[63] I. Ivančev-Tumbas. The fate and importance of organics in drinking water treatment: a review. Environ. Sci. Pollut. Res 21(20)11794–11810, 2014. https://doi.org/10.1007/s11356-014-2894-8

[64] B. Teychene, G. Collet, H. Gallard. Modeling of combined particles and natural organic matter fouling of ultrafiltration membrane. J. Membr. Sci 505 (August) 185–193. https://doi.org/10.1016/j.memsci.2015.07.024

[65] X. Zhang, L. Fan, F. A. Roddick. Effect of feedwater pre-treatment using UV / H 2 O 2 for mitigating the fouling of a ceramic MF membrane caused by soluble algal organic matter. J. Membr. Sci 493 (2015) 683–689.

[66] E. Iritani, N. Katagiri. Developments of blocking filtration model in membrane filtration. KONA Powder Part. J.2016 (33) 179–202. DOI: 10.14356/kona.2016024

[67] N. Shamsuddin, D. B. Das, V. M. Starov. Filtration of natural organic matter using ultrafiltration membranes for drinking water purposes: Circular cross-flow compared with stirred dead end flow. Chem. Eng. J 276 (August) 331–339, 2016. https://doi.org/10.1016/j.cej.2015.04.075

[68] M. A. Javeed, K. Chinu, H. K. Shon, S. Vigneswaran. Effect of pre-treatment on fouling propensity of feed as depicted by the modified fouling index (MFI) and cross-flow sampler-modified fouling index (CFS-MFI). Desalination 238 (1–3) 98–108, 2009. https://doi.org/10.1016/j.desal.2008.01.040

[69] T. O. Mahlangu, E. M. V Hoek, B. B. Mamba, A. R. D. Verliefde. Influence of organic, colloidal and combined fouling on NF rejection of NaCl and carbamazepine: Role of solute-foulant-membrane interactions and cake-enhanced concentration polarisation. J. Membr. Sci 471 (July) 35–46, 2014. https://doi.org/10.1016/j.memsci.2014.07.065

[70] S. Meylan, F. Hammes, J. Traber, E. Salhi, U. von Gunten, W. Pronk. Permeability of low molecular weight organics through nanofiltration membranes. Water Res 41 (17) 3968–3976, 2007. DOI: 10.1016/j.watres.2007.05.031

[71] T. Jiang, U. Skyllberg, E. Björn.N.W.Green, J. Tang, D. Wang, J. Gao, C. Lia. Characteristics of dissolved organic matter (DOM) and relationship with dissolved mercury in Xiaoqing River-Laizhou Bay estuary, Bohai Sea, China. Environ. Pollut 223 (2017) 19–30. https://doi.org/10.1016/j.envpol.2016.12.006

[72] C. Li, W. Sun, Z. Li, X. Ao, S. Li. Ceramic nanocomposite membranes and membrane fouling: A review. Water Res 175(2020) 115674. https://doi.org/10.1016/j.watres.2020.115674